Copyright Information

This is a post-peer-review, pre-copyedit version of the following paper

The final authenticated version is available online at:
http://ieeexplore.ieee.org/abstract/document/8232288/

You are welcome to cite this work using the following bibliographic information:

```
BibTeX

@inproceedings{simetti2017robust,
  title={ROBUST project: Control framework for deep sea mining
      exploration},
  author={Simetti, Enrico and Wanderlingh, Francesco and Casalino,
      Giuseppe and Indiveri, Giovanni and Antonelli, Gianluca},
  booktitle={OCEANS--Anchorage, 2017},
  pages={1--5},
  year={2017},
  publisher={IEEE}
}
```

ROBUST project: Control Framework for Deep Sea Mining Exploration

Enrico Simetti*†, Francesco Wanderlingh*†, Giuseppe Casalino*†, Giovanni Indiveri*‡, Gianluca Antonelli*§

*Interuniversity Research Center on Integrated Systems for the Marine Environment
Via Opera Pia 13, 16145 Genova, Italy, Email: enrico.simetti@unige.it
†DIBRIS, University of Genova, Via Opera Pia 13, 16145 Genova, Italy
‡DII, University of Salento, Via per Monteroni, 73100 Lecce, Italy
§University of Cassino and Southern Lazio, Via Di Biasio 43, 03043, Cassino, Italy

Abstract—This paper presents the control framework under development within the ROBUST Horizon 2020 project, whose goal is the development of an autonomous robotic system for the exploration of deep-sea mining sites. After a bathymetric survey of the initial zone of interest, the robotized system selects a subarea deemed to have the most chances of containing a manganese nodule field and proceeds with a detailed low altitude survey. Whenever a possible nodule is found, it performs an in-situ measurement through laser induced spectroscopy. To do so, the underwater vehicle must first land on the seafloor, with a certain precision to allow a subsequent fixed-based manipulation, bringing its manipulator endowed with the laser system in the position to carry out the measurement. The work reports the developed control architecture and the simulation results supporting it.

I. INTRODUCTION

Securing reliable, sustainable and undistorted supply of raw materials is of growing concern. This is true especially in Europe, since the biggest producers and exporters of raw materials are found outside of Europe as identified in a report [1]. In recent years, there has been a growing interest in moving to the deep sea for raw materials, however cost effective and environmentally friendly exploration technologies remain key issues.

Two prominent issues are of great importance with respect to rapid and robust exploration and identification of deep sea mining sites. First and foremost is the means to 3D map the seabed in a quick and efficient manner, using high resolution sensors and at the same time being able to cover a large terrain with little supervision. It is evident that the mid ocean ridge, where massive sulphide sites could potentially be found, is to a very large extend unmapped, with only 0.1% mapped to this day [2]. The second issue is the element identification of the minerals found in these mining sites. Current practice dictates that a Remotely Operated Vehicle (ROV) along with a surface support vessel (SSV) are employed for mineral sampling from the sea bed to the SSV and further on to shore station for analysis and element identification. The cost savings of using an Autonomous Underwater Vehicle (AUV) for the same task, instead of a ROV, can reach up to 85% for a full 24 hour shift operation and 2 AUVs in tandem [3]. Although the former exercise [3] has been performed for the oil & gas industry, it clearly demonstrates the cost savings of using an AUV instead of an ROV, to perform the same task.

In this sense there is a need to develop an autonomous, reliable, cost effective technology to map vast terrains, in terms of mineral and raw material contents which will aid in reducing the cost of mineral exploration, currently performed by ROVs and dedicated SSVs and crew. Furthermore there is a need to identify, in an efficient and non-intrusive manner (minimum impact to the environment), the most rich mineral sites. Such a technology would aid the seabed mining industry, reduce the cost of exploration and especially the detailed identification of the raw materials contained in a mining sites and enable targeted mining only of the most rich resources existing.

The ROBUST project [4], funded by the EU commission under the Horizon 2020 programme, aims to tackle the aforementioned issue by developing sea bed in-situ material identification through the fusion of two technologies, namely laser-based element-analysing capability merged with AUV technologies for sea bed 3D mapping. The underwater robotic laser process is the Laser Induced Breakdown Spectroscopy (LIBS), used for identification of materials on the sea bed. The envisioned mission of the ROBUST AUV consists of the following major steps:

1) The AUV dives to the preprogrammed altitude (around 30-50 m) and follows a pre-programmed lawnmower path over a pre-defined *working area*, in order to gather MBES (Multi beam echo sounder) data.

2) The MBES data is processed on board to create bathymetric and backscatter maps of the area. On the basis of these maps, the coordinates of the area with the estimated highest probability of manganese nodules is given to the AUV control software (called the *image box area*).

3) The AUV proceeds to the given coordinates, and starts a new lawnmower survey, this time at about 2 m altitude. In this survey, a camera is used in real-time to find features similar to a manganese nodule within the image.

4) At the end of the survey, if not enough features similar to manganese nodules are found, the AUV leaves the image box area and proceeds to the second-best area, and so forth. Conversely, the area is deemed worthy to be in-situ analysed. Therefore, the AUV goes back to

the start of the image box survey area, with the goal of analysing the nodules.

5) The first time the AUV identifies a nodule, AUV begins the procedure for its analysis.

This work presents the control framework currently being developed by ISME (Interuniversity Research Center on Integrated System for the Marine Environment) to let the AUV being capable of executing the aforementioned autonomous mission. The proposed control framework is an evolution of the one first developed for the TRIDENT project [5], and it is now based on the task priority kinematic inversion procedure presented in [6] developed during the MARIS project [7], [8]. This framework is currently being expanded both within the ROBUST project and the DexROV project [9], [10].

Two different options are currently being considered for the in-situ analysis of the nodule:

- The AUV hovers over the nodule, and the manipulator carrying the LIBS is moved toward the nodule to perform the measurement, initially using vision as feedback and then using a proximity sensor to guide the end-effector on top of the nodule.
- The AUV lands in front of the nodule, a 3D laser-scanning procedure creates a 3D model of the nodule, and on the basis of that reconstruction the manipulator, acting as a fixed base one, moves the LIBS in the position to perform the measurement.

In this paper, a framework that supports both options will be presented, however simulation results will be presented only for the second case. In particular, section II recalls the basic concepts of the task priority framework, section III shows the simulation results for the landing and in-situ inspection, and finally section IV draws some conclusions and future line of development.

II. TASK PRIORITY CONTROL FRAMEWORK

This section recalls the main concepts of the task priority framework currently used within the ROBUST project and implemented within the kinematic control layer. The interested reader can find a deeper discussion in [11].

A. Core Concepts

The first key concept is the definition of the control objectives of the system. Let us consider the configuration vector $\boldsymbol{c} = \begin{bmatrix} \boldsymbol{\eta} & \boldsymbol{q} \end{bmatrix}^T \in \mathbb{R}^n$, which describes the degrees of freedom (DOF) of the system. Then, a configuration dependent scalar variable $x(\boldsymbol{c})$ is required to achieve an *equality* when, for $t \to \infty$, the following condition needs to be achieved:

$$x(\boldsymbol{c}) = x_0, \tag{1}$$

or *inequality control objective* when, for $t \to \infty$, the following condition needs to be achieved:

$$x(\boldsymbol{c}) \geq x_{min} \text{ and/or } x(\boldsymbol{c}) \leq x_{max}, \tag{2}$$

where the min and max subscripts indicate a minimum and maximum value respectively.

Control tasks are the tools to achieve control objectives. Simply put, a *reactive control task* is the requirement of having the task velocity $\dot{x} = \boldsymbol{g}^T \dot{\boldsymbol{y}}$ as much as possible equal to the desired one $\dot{\bar{x}}$, where $\dot{\boldsymbol{y}} = \begin{bmatrix} \boldsymbol{v} & \dot{\boldsymbol{q}} \end{bmatrix}^T \in \mathbb{R}^n$ is the system velocity vector and $\boldsymbol{g} \in \mathbb{R}^n$ is the Jacobian of the task. The desired velocity is expressed in terms of a *feedback* control law, as for example a simple proportional law:

$$\dot{\bar{x}} \triangleq \gamma(x^* - x), \gamma > 0. \tag{3}$$

where x^* is equal to x_0 for equality control objectives, while it is any point inside the validity region for inequality ones.

As control objectives may or may not be relevant in a given situation, activation functions are introduced to dynamically tuning the system's behavior at runtime, for instance on the basis of sensory data. For example, considering the problem of maintaining a minimum altitude from the sea floor, then the related task would be relevant only when the vehicle is close to the sea floor. This task should not over-constrain the UVMS whenever sufficiently far away.

Motivated by the above considerations, let us define a prototype for activation functions such that:

$$a(x) = a^i(x), \tag{4}$$

where $a^i(x) \in [0, 1]$ is a continuous sigmoid function of a scalar objective variable x, whose value is zero within the validity region of the associated control objective.

In addition to reactive tasks, the framework supports non-reactive ones. A task is called non-reactive when it is defined directly in the velocity space of the task. For example, consider the case where a human operator wants to control the end-effector by generating velocity references through a joystick. In such a case, there is no control objective associated with the control task, because there is not a position to reach. In fact, the reference rate is generated by the user, rather than being the output of a feedback control loop as in (3).

Once the control objectives and tasks have been defined, a priority level must be assigned to each of them, and more than one can be assigned to the same priority level. This procedure leads to the definition of the following matrices and vector, assuming m_k control tasks are assigned at a given k-th priority level:

- $\dot{\bar{\boldsymbol{x}}}_k \in \mathbb{R}^{m_k}$ is the reference vector, obtained stacking each scalar reference;
- $\boldsymbol{A}_k \in \mathbb{R}^{m_k \times m_k}$ is the diagonal activation matrix, where each diagonal element is the activation function (4);
- $\boldsymbol{J}_k \in \mathbb{R}^{m_k \times n}$ is the Jacobian, obtained by stacking each Jacobian row $\boldsymbol{g}^T$.

With these definitions, the control problem is to find the system's velocity reference vector $\dot{\bar{\boldsymbol{y}}}$ complying with the aforementioned priority requirements. In order to compute such a vector, a Task Priority Inverse Kinematic (TPIK) procedure has been proposed in [6]. Here, it would suffice to describe the single regularization and optimization step, which unfolds iteratively taking into account all lower priority tasks. The

manifold of solutions at the k level is:

$$S_k \triangleq \left\{ \arg \text{R-} \min_{\dot{\boldsymbol{y}} \in S_{k-1}} \left\| \boldsymbol{A}_k(\dot{\bar{\boldsymbol{x}}}_k - \boldsymbol{J}_k \dot{\boldsymbol{y}}) \right\|^2 \right\}, \ k = 1, 2, \ldots, N, \tag{5}$$

where S_{k-1} is the manifold of solutions of all the previous tasks in the hierarchy, $S_0 \triangleq \mathbb{R}^n$, and N is the total number of priority levels. These minimization problems can be affected by algorithmic singularities due to the activation matrix $\boldsymbol{A}_k$, creating discontinuities in the control variables. To avoid that, a special regularization mechanism has been used during the minimization process, and this fact is underlined by the notation R- $\min$. A detailed explanation of these problems and the related regularization mechanism is duly reported in [6], together with the definition of the special pseudo inverse operator $(\cdot)^{\#,\boldsymbol{A},\boldsymbol{Q}}$ and will be omitted here.

The overall TPIK methodology (named *iCAT task priority framework*) results in the following algorithm, initialized with

$$\boldsymbol{\rho}_0 = \boldsymbol{0}, \quad \boldsymbol{Q}_0 = \boldsymbol{I}, \tag{6}$$

then for $k = 1, \ldots, N$

$$\begin{aligned}
\boldsymbol{W}_k &= \boldsymbol{J}_k \boldsymbol{Q}_{k-1} (\boldsymbol{J}_k \boldsymbol{Q}_{k-1})^{\#,\boldsymbol{A}_k,\boldsymbol{Q}_{k-1}}, \\
\boldsymbol{Q}_k &= \boldsymbol{Q}_{k-1}(\boldsymbol{I} - (\boldsymbol{J}_k \boldsymbol{Q}_{k-1})^{\#,\boldsymbol{A}_k,\boldsymbol{I}} \boldsymbol{J}_k \boldsymbol{Q}_{k-1}), \\
\boldsymbol{\rho}_k &= \boldsymbol{\rho}_{k-1} \\
&\quad + \text{Sat}\left(\boldsymbol{Q}_{k-1}(\boldsymbol{J}_k \boldsymbol{Q}_{k-1})^{\#,\boldsymbol{A}_k,\boldsymbol{I}} \boldsymbol{W}_k \left(\dot{\bar{\boldsymbol{x}}}_k - \boldsymbol{J}_k \boldsymbol{\rho}_{k-1}\right)\right),
\end{aligned} \tag{7}$$

where the $\text{Sat}(\cdot)$ function implements the management of control variable saturations suggested in [12]. The interested reader can find all the relevant details of this procedure in [6], where a comparison with other task priority frameworks such as [13], [14], [15] is given.

B. Actions

An *action* is defined as a given list of prioritized control objectives and control tasks. The simplest one that can be defined for the ROBUST system is the following one

1) [R, I, S] Vehicle minimum altitude;
2) [R, I, S] Vehicle obstacle avoidance;
3) [R, I, S] Vehicle horizontal attitude;
4) [R, I, P] Vehicle auto-heading;
5) [R, I, AD] Vehicle position (x, y and depth);

which defines a *safe navigation to a waypoint* action. The following compact notation has been used

- [R/NR, I/E, C/S/P/AD/O] Name of the task/objective;

where

- R/NR specifies if the task is reactive or non-reactive;
- I/E specifies if the task is of inequality or equality type;
- C/S/P/AD/O specifies if the category of the task, i.e. constraint, safety, prerequisite, action-defining, optimization.

As mentioned in the introduction, the in-situ measurement is carried out by landing on the sea floor and then doing a fixed based manipulation to bring the LIBS close to the nodule to be inspected. The landing is performed through two consecutive actions. The first one, named $\mathcal{A}_a$ has the goal of stabilizing

the distance to the nodule and its alignment, and is represented by the following list of objectives:

1) [R, I, S] Vehicle minimum altitude.
2) [R, I, S] Vehicle horizontal attitude;
3) [R, I, AD] Vehicle longitudinal alignment to the nodule;
4) [R, I, AD] Vehicle distance to the nodule;

After the alignment and distance errors are within some established thresholds, the landing action $\mathcal{A}_l$ can actually take place

1) [R, I, S] Vehicle horizontal attitude;
2) [R, I, P] Vehicle longitudinal alignment to the nodule;
3) [R, I, P] Vehicle distance to the nodule;
4) [R, E, AD] Vehicle altitude.

As can be seen, in the first action there is an inequality control objective to maintain a *minimum altitude* from the seafloor, to avoid landing in an incorrect position. In the second action, the minimum altitude objective is removed and replaced by an *equality* objective to regulate the altitude to zero and achieve landing. Furthermore, the distance and alignment to the nodule objectives remain active, although they have a different priority with respect to those concerning the altitude. These two actions, in a strict sequence, allow to land in the correct position.

Finally, the fixed based manipulation action $\mathcal{A}_m$ is represented by:

1) [R, I, S] Arm joint limits;
2) [R, I, P] Arm manipulability;
3) [R, E, AD] End-effector linear position control;
4) [R, E, AD] End-effector angular position control;
5) [R, I, O] Arm preferred shape;

C. Missions

Following the general description of the task priority control procedure and the examples given in the previous section, the following aspects can be highlighted:

- Actions are generally constituted by the same safety objectives, while they usually differ for those defined as action-defining. For example, the equality control objective to regulate the vehicle altitude clearly identifies a landing action, while maintaining an horizontal attitude is desirable both when landing and when navigating to a waypoint.
- A mission plan can be constructed as a graph of actions, where the actions are the nodes while the arcs are logic alternatives.
- Moreover, transitions from an action to another one located at the end of a selected arc, should be smoothly activated.

For the sake of argument, let us imagine a unified list made up of all control objectives of two actions $\mathcal{A}_1$ and $\mathcal{A}_2$. It is easy to imagine how, by a simple removal of some of the control objectives, the two initial sets can be easily determined. To do so, activation functions in the form of (4) are modified as:

$$a(x, \boldsymbol{p}) = a^i(x) a^p(\boldsymbol{p}), \tag{8}$$

where $a^p(\boldsymbol{p}) \in [0,1]$ is a continuous sigmoid function of a vector of parameters $\boldsymbol{p}$ external to the control task itself. In particular, $a^p(\boldsymbol{p})$ can be conveniently parametrized by the two subsequent actions, as well as the time elapsed from the start time of the current action, to obtain the desired activation/deactivation smooth transition function between sets of objectives.

III. SIMULATION RESULTS

In this section we present some simulation results of the proposed kinematic control strategy. Some screenshots of the AUV executing the landing procedure and the in-situ LIBS measurement mission are shown in Figure 1.

The parameters used for the simulation are the following ones.

- Dynamic simulation and dynamic control loops were running at 1 kHz frequency, and dynamic control was based on separate independent PI loops, tuned around the nominal inertia of the links and vehicle.
- Vehicle generalized forces were saturated at 400 N on the surge axis of the vehicle, and 300 N along the sway and heave axes; vehicle generalized torques was saturated at 150 Nm on each axes.
- Each arm link inertia was modelled taking into account mass and reduction gears and arm torques were saturated at $\begin{bmatrix} 45 & 125 & 50 & 50 & 10 & 10 & 4 \end{bmatrix}$ Nm (values are taken from the Graal Tech UMA commercial arm).
- Kinematic control loop was running at 100 Hz frequency, based on the proposed task priority approach with velocity saturations.
- The considered velocity saturations were 1 rad/s for the arm joints, 0.2 m/s for the vehicle linear velocity and 0.2 rad/s for the vehicle angular velocities.

To stress the system, the simulation is initialized with the vehicle very close to the seafloor. The initial action is $\mathcal{A}_a$ and guarantees a minimum altitude between 0.5 m and 1 m, as can be seen from Fig. 2(b). Furthermore, the alignment and the distance to the nodule errors are reduced below predefined thresholds. This can be seen by looking at the activation functions of the nodule alignment and nodule distance control objectives plotted in Fig. 2(a), which decrease and are less than 1. Then, at about $t = 2.3$ s, the system changes from action $\mathcal{A}_a$ to $\mathcal{A}_l$, activating smoothly the new control objectives to execute the landing, and deactivating those that are not anymore relevant. Finally, around $t = 7.2$ s , the UVMS switches from action $\mathcal{A}_l$ to $\mathcal{A}_m$. In this case the transition is not smooth, to turn off immediately the thrusters of the vehicle. Once $\mathcal{A}_m$ is active, the manipulator starts moving to perform the in-situ measurement of the nodule. Figures 2(c) and 2(d) show the reference joint velocities and vehicle velocities generated by the TPIK procedure during the manoeuvre.

IV. CONCLUSIONS

This paper has presented the general control framework employed within the ROBUST H2020 project. In particular,

the core concepts of control objectives, control task and actions have been presented.

The most crucial phase of the ROBUST mission has been presented through accurate hydrodynamic simulations. In particular, after a possible manganese nodule has been individuated, the UVMS adjusts its position and performs a landing action, with the goal of having the nodule within the working area of the manipulator. Once the landing has been accomplished, a fixed based manipulation action is performed, bringing the arm's end-effector with the LIBS within the required distance from the nodule to perform the in-situ measurement.

Current works are focusing on the software implementation of the proposed approach, for the upcoming engineering tests scheduled for 2018. Further theoretical insights on how to tune the different gains and parameters of the TPIK procedure to be compatible with the underlying dynamic control layer are also on-going.

REFERENCES

[1] (2014) Report on critical raw materials for the eu. [Online]. Available: https://ec.europa.eu/growth/sectors/raw-materials/specific-interest/critical_it

[2] (2017) Mid ocean ridge exploration facts. [Online]. Available: http://oceanexplorer.noaa.gov/facts/mid-ocean-ridge.html

[3] (2017) The efficiencies of low logistics, man-portable auvs for shallow water survey operations. [Online]. Available: http://www.subseauk.com/documents/ncs%20survey.pdf

[4] "ROBUST website," http://eu-robust.eu, 2016, [Online; accessed 25-October-2016].

[5] E. Simetti, G. Casalino, S. Torelli, A. Sperindé, and A. Turetta, "Floating underwater manipulation: Developed control methodology and experimental validation within the trident project," *Journal of Field Robotics*, vol. 31, no. 3, pp. 364–385, May 2014.

[6] E. Simetti and G. Casalino, "A novel practical technique to integrate inequality control objectives and task transitions in priority based control," *Journal of Intelligent & Robotic Systems*, vol. 84, no. 1, pp. 877–902, apr 2016.

[7] G. Casalino, M. Caccia, S. Caselli, C. Melchiorri, G. Antonelli, A. Caiti, G. Indiveri, G. Cannata, E. Simetti, S. Torelli, A. Sperindè, F. Wanderlingh, G. Muscolo, M. Bibuli, G. Bruzzone, E. Zereik, A. Odetti, E. Spirandelli, A. Ranieri, J. Aleotti, D. Lodi Rizzini, F. Oleari, F. Kallasi, G. Palli, U. Scarcia, L. Moriello, and E. Cataldi, "Underwater intervention robotics: An outline of the italian national project MARIS," *Marine Technology Society Journal*, vol. 50, no. 4, pp. 98–107, jul 2016.

[8] E. Simetti and G. Casalino, "Manipulation and transportation with cooperative underwater vehicle manipulator systems," *IEEE Journal of Oceanic Engineering*, pp. 1–18, 2016.

[9] P. A. Di Lillo, E. Simetti, D. De Palma, E. Cataldi, G. Indiveri, G. Antonelli, and G. Casalino, "Advanced ROV autonomy for efficient remote control in the DexROV project," *Marine Technology Society Journal*, vol. 50, no. 4, pp. 67–80, jul 2016.

[10] E. Simetti, F. Wanderlingh, G. Casalino, G. Indiveri, and G. Antonelli, "DexROV project: Control framework for underwater interaction tasks," in *MTS/IEEE OCEANS 17*, Aberdeen, Scotland, 2017.

[11] G. Casalino, E. Simetti, and F. Wanderlingh, "Robotized underwater interventions," in *Sensing and Control for Autonomous Vehicles: Applications to Land, Water and Air Vehicles*, T. I. Fossen, K. Y. Pettersen, and H. Nijmeijer, Eds. Cham: Springer International Publishing, 2017, pp. 365–386.
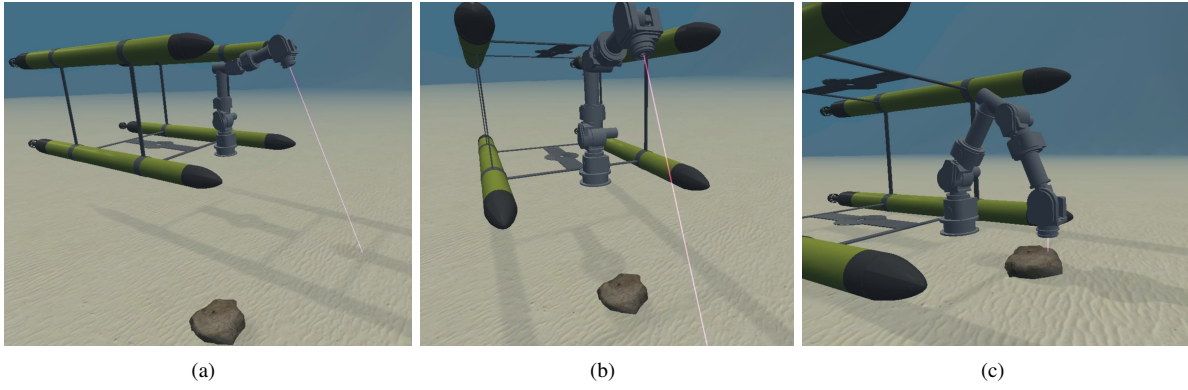
(a)   (b)   (c)

Fig. 1. Screenshots of the AUV as it performs the landing and then the LIBS measurement.
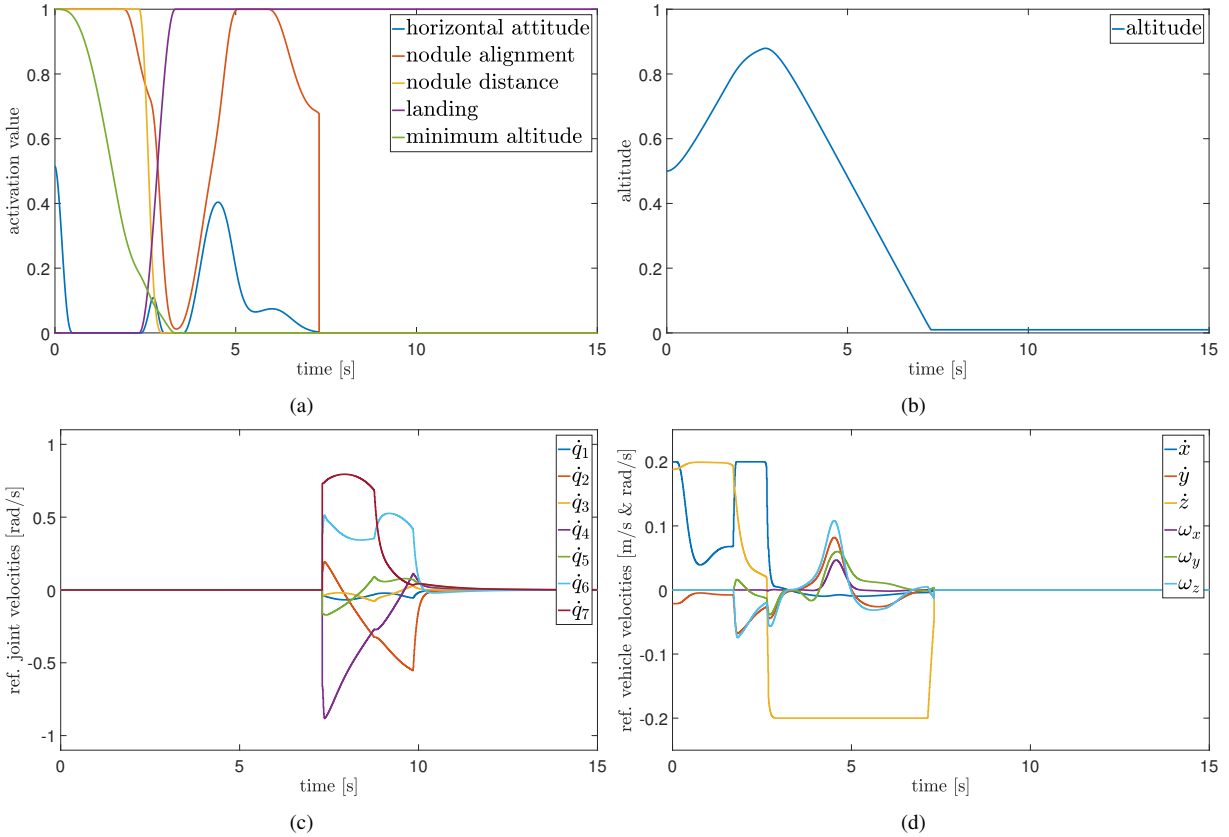

(a)   (b)

(c)   (d)

Fig. 2. Simulation results: (a) the activation values of the vehicle-related tasks during the landing phases, (b) the altitude from the seafloor (c) vehicle reference velocities (saturation value at 0.2 rad/s and 0.2 m/s) (d) the arm joint velocities (saturation value at 1 rad/s)

[12] G. Antonelli, G. Indiveri, and S. Chiaverini, "Prioritized closed-loop inverse kinematic algorithms for redundant robotic systems with velocity saturations," in *Intelligent Robots and Systems, 2009. IROS 2009. IEEE/RSJ International Conference on*. IEEE, 2009, pp. 5892–5897.

[13] O. Kanoun, F. Lamiraux, and P. B. Wieber, "Kinematic control of redundant manipulators: generalizing the task-priority framework to inequality task," *IEEE Transactions on Robotics*, vol. 27, no. 4, pp. 785–792, 2011.

[14] A. Escande, N. Mansard, and P.-B. Wieber, "Hierarchical quadratic programming: Fast online humanoid-robot motion generation," *The International Journal of Robotics Research*, vol. 33, no. 7, pp. 1006–1028, 2014.

[15] S. Moe, G. Antonelli, A. R. Teel, K. Y. Pettersen, and J. Schrimpf, "Set-based tasks within the singularity-robust multiple task-priority inverse kinematics framework: General formulation, stability analysis, and experimental results," *Frontiers in Robotics and AI*, vol. 3, p. 16, 2016.